Nonlinear refraction of hard x rays

A. Fratalocchi,[1,2] C. Conti,[2] G. Ruocco,[2,3] and F. Sette[4]
[1]*Research Center Enrico Fermi, Via Panisperna 89/A, I-00184 Roma, Italy*
[2]*Research Center SOFT INFM-CNR, c/o University of Rome "Sapienza," I-00185 Roma, Italy*
[3]*Department of Physics, University of Rome "Sapienza," I-00185 Roma, Italy*
[4]*European Synchrotron Radiation Facility, Boîte Postale 220, 38043 Grenoble, France*
(Received 8 February 2008; revised manuscript received 30 April 2008; published 25 June 2008)

We study the nonlinear refraction of x rays in highly ionized condensed matter by using a classical model of a cold electron plasma in a lattice of still ions coupled with Maxwell equations. By employing a group-theoretical technique, we reduce the governing equations of the system to an integrable set of nonlinear ordinary differential equations, discussing the existence and stability of nonlinear waves. This allows us to define the effective Kerr coefficient n_2 at x rays. With reference to real-world crystalline materials (B, C, Li, and Na), we consider *beam self-defocusing* and predict that nonlinear processes become comparable to the linear ones for focused beams with powers on the order of mc^3/r_0 (≈ 10 GW), the *classical electron power*. As a consequence, nonlinear phenomena are expected to largely affect imaging experiments in currently exploited x-ray free-electron lasers and in their future developments.

DOI: 10.1103/PhysRevB.77.245132 PACS number(s): 41.50.+h, 52.25.Os, 61.05.cp

I. INTRODUCTION

Understanding nonlinear processes at the smallest accessible spatiotemporal scale is at the frontier of modern research. In this respect, the new generation of x-ray free-electron lasers (FELs) will open unprecedented possibilities such as, for example, nonlinear optics in the x-ray region (see, e.g., Refs. 1 and 2). The new x-ray FELs are expected to deliver femtosecond pulses in the wavelength range of 0.05–1 nm with peak power greater than 100 GW (see, e.g., Ref. 3), corresponding to intensities up to 10^{23} W cm^{-2} for beams focused down to 10 nm spot size. Even if we do not take into account relativistic effects and particle production (expected at intensities of $\approx 10^{26}$ W cm^{-2}; see, e.g., Refs. 4 and 5), the underlying fundamental physical processes are in many respects unknown and of great interest. Photons at the atomic-scale wavelength ($\lambda \approx 0.1$ nm) have macroscopic propagation lengths in condensed materials (even when photoelectric absorption is considered) and are sensitive to the granular structure of matter.[6–11] In this respect, the physics of high intensity x-ray beams have to take into account nonlinear effects accumulating along large propagation distances in inhomogeneous environments. From a general perspective, high-fluence x-ray photon bursts rapidly ionize the material, and the basic nonlinear processes are due to the hydrodynamics of the generated electron plasma (see, e.g., Refs. 1, 4, and 12–15 and references therein). At hard x-ray wavelengths, the linear refractive index (due to plasma) differs from unity by an amount δ that is on the order of 10^{-5} (see Sec. II B).

In this paper, we detail the nonlinear contribution to δ, which is an issue of high relevance in preparation of the future science of x-ray FEL. In the early days of nonlinear optics, Jha and Warke[13] and Bloembergen[6] reported on similar analyses; here we extend those works in a twofold way: (i) We largely generalize previous results beyond the lowest-order approximation by considering realistic aggregates of atomic systems. (ii) We particularize to real-world experiments with reference to the expected performances of the modern x-ray FEL in terms of power, losses, and beam divergence.

Within a purely classical formulation, we show that the nonlinear contribution to the index of refraction, which is expressed in terms of the effective Kerr coefficient n_2 (Ref. 17) as $n_2 I$ for low intensity I, becomes on the order of the plasma linear refractive index δ for diffraction-limited focused beams with powers on the order of 10 GW (a basically wavelength-independent result, even when photoabsorption is included). With reference to current experiments performed at FLASH,[18] this effect can be observed for tightly focused beams (even if not at the diffraction limit). We evaluate the third-order nonlinear susceptibility of the x-ray induced plasma, demonstrating the existence of stable nonlinear waves. A realistic experiment is then suggested to quantify the self-defocusing of an x-ray beam in real crystals (B, C, Li, and Na).

This paper is organized as follows: Section II A introduces the nonlinear equations governing the system. Section II B deals with the calculation of the spectrum of the linear system by means of a group-theoretical technique. We exemplify our spectral analysis for two typical periodic arrangements, the simple-cubic (Sec. II B 1) and the face-centered-cubic (Sec. II B 2) lattices, deriving a reduced, integrable, nonlinear set of evolution equations in Sec. II C. Section II D contains a discussion on nonlinear waves and their stability, while Sec. II E deals with the nonlinear Kerr coefficient n_2 and its implications at x rays. Finally, Sec. II F presents a realistic experimental realization with a discussion on the effect of losses.

II. THEORY

A. Governing equations

X-ray propagation is described by Maxwell equations coupled with the hydrodynamic equations for a plasma of free electrons:[1,12]

$$\nabla \times \mathbf{h} = \mathbf{j} + \epsilon_0 \partial_t \mathbf{e},$$

$$\nabla \times \mathbf{e} = -\mu_0 \partial_t \mathbf{h},$$

$$\partial_t n + \nabla \cdot (n\mathbf{v}) = 0,$$

$$(\partial_t + \mathbf{v} \cdot \nabla)\mathbf{v} + \frac{q}{m}(\mathbf{e} + \mu_0 \mathbf{v} \times \mathbf{h}) = 0, \tag{1}$$

where $\mathbf{e}$ and $\mathbf{h}$ are the time-dependent electromagnetic fields, $\mathbf{v}$ is the electron mean velocity, and $\mathbf{j}=-qn\mathbf{v}$ is the current generated by the charge density $q(n-n_0)$, with $n(\mathbf{r})$ and $n_0(\mathbf{r})$ as the particle densities of electrons and ions, respectively. We make the assumption that high-energy photons instantaneously (i.e., at attosecond scales) ionize the material, so that the electromagnetic field propagates in a periodically distributed *cold* plasma whose evolution, governed by the last two equations in Eq. (1), affects the whole x-ray pulse during propagation. This implies that in this analysis we neglect temporal effects due to delayed complete ionization with respect to x-ray pulse arrival (see, e.g., Fig. 1 of Ref. 18); indeed we focus here on the role of nonlinear refraction in the forward beam scattering, which is expected in the proximity of the peak pulse, and we will investigate temporal effects in a future work. The ion cores with density n_0, in other terms, are assumed to be "frozen;" they only form the crystal lattice. In our picture, the x-ray free-electron laser (XFEL) electric-field amplitude is sufficiently high to heavily perturb the nuclear electric field and induce multiple ionization.

By generalizing the formalism of the coupled-mode theory,[19] we reduce Eq. (1) to an integrable set of ordinary differential equations. We begin by expanding the current as $\mathbf{j}=\mathbf{j}_L+\mathbf{j}_\Delta$, where $\mathbf{j}_L$ is a linear contribution and $\mathbf{j}_\Delta$ is an arbitrary nonlinear term. In the linear regime $\mathbf{j}=\mathbf{j}_L$ and the Fourier domain ($\partial_t \rightarrow -i\omega$), Eq. (1) is written in the *canonical* form

$$\nabla \times \tilde{\mathbf{H}} = -i\omega\epsilon_0\left(1 - \frac{\omega_\alpha^2}{\omega^2}\right)\tilde{\mathbf{E}}, \quad \nabla \times \tilde{\mathbf{E}} = i\omega\mu_0\tilde{\mathbf{H}}, \tag{2}$$

with $\omega_\alpha^2 = q^2 n_0 / m\epsilon_0$.

B. Normal modes of the canonical structure

Under typical experimental conditions ($\lambda \approx 0.1$ nm and $\langle n_0 \rangle \approx 10^{30}$ m^{-3}, with $\langle\ \rangle$ denoting a mean value), $\omega_\alpha^2/\omega^2 \approx 10^{-5}$. The term $1-\delta$, with $\delta=\omega_\alpha^2/\omega^2$, behaves as an effective periodic dielectric constant $\epsilon_r(\mathbf{r})$, whose period is settled by the crystal lattice constant a. The spectrum of such a periodic system is then found by applying the Floquet-Bloch theorem.[20] The latter states that the eigenmodes in Eq. (2) are Bloch modes $\tilde{\mathbf{E}}_\mathbf{k}$ and $\tilde{\mathbf{H}}_\mathbf{k}$, with

$$\tilde{\mathbf{H}}_\mathbf{k}(\mathbf{r}) = \tilde{\mathbf{u}}_\mathbf{k}(\mathbf{r})\ \exp(i\mathbf{k} \cdot \mathbf{r}),$$

$$\tilde{\mathbf{E}}_\mathbf{k}(\mathbf{r}) = \tilde{\mathbf{w}}_\mathbf{k}(\mathbf{r})\ \exp(i\mathbf{k} \cdot \mathbf{r}), \tag{3}$$

where $\mathbf{k}$ is the Bloch wave number. Magnetic modes $\tilde{\mathbf{H}}_\mathbf{k}$ are solution of the self-adjoint eigenvalue problem

$$\mathcal{L}_H \tilde{\mathbf{H}}_\mathbf{k} = \left(\frac{\omega}{c}\right)^2 \tilde{\mathbf{H}}_\mathbf{k}, \tag{4}$$

with

$$\mathcal{L}_H = \nabla \times \frac{1}{\epsilon_0 \epsilon_r} \nabla\ \times, \tag{5}$$

and $\omega(\mathbf{k})$ as the medium dispersion relation. Actually, only magnetic modes are to be calculated since eigenmodes $\tilde{\mathbf{E}}_\mathbf{k}$ depend on $\tilde{\mathbf{H}}_\mathbf{k}$ via

$$i\omega\epsilon_0\epsilon_r \tilde{\mathbf{E}}_\mathbf{k} = \nabla \times \tilde{\mathbf{H}}_\mathbf{k}. \tag{6}$$

Owing to the lattice periodicity, eigenmode (3) and eigenvalues $\omega(\mathbf{k})$ are periodic in the reciprocal (wave-vector) space for $\mathbf{k}=\mathbf{k}+\mathbf{G}$, where $\mathbf{G}=\mathbf{l}\cdot\mathbf{b}$ is an arbitrary translation in the reciprocal lattice with $\mathbf{l}$ as a vector of integers and $\mathbf{b}$ given by $\mathbf{a}_i \cdot \mathbf{b}_j = 2\pi\delta_{ij}$ ($\mathbf{a}_i$ is the vector of the unit cell of the lattice in the direct space $\mathbf{r}$). Envelopes $\tilde{\mathbf{u}}_{\mu\mathbf{k}}$ and $\tilde{\mathbf{w}}_{\mu\mathbf{k}}$, conversely, are periodic for $\mathbf{r}=\mathbf{r}+\mathbf{a}$. The electromagnetic spectrum $\mathcal{S}$ of the canonical structure is therefore given by $\mathcal{S}=\{\tilde{\mathbf{H}}_\mathbf{k}, \tilde{\mathbf{E}}_\mathbf{k}, \omega(\mathbf{k})\}$, with eigenvalues $\omega(\mathbf{k})$ defining the medium dispersion relation.

Due to the smallness of the dielectric perturbation ω_α^2/ω^2, the spectrum $\mathcal{S}=\{\tilde{\mathbf{H}}_\mathbf{k}, \tilde{\mathbf{E}}_\mathbf{k}, \omega(\mathbf{k})\}$ of the canonical structure is completely determined by the representation theory of space groups.[20,21] The latter has been successfully employed to solve classification problems in optics,[20,22] as well as to calculate the spectrum of scalar operators in solid-state physics, chemistry, and biology.[21,23] Here we generalize these analyses to the vectorial operator $\mathcal{L}_H$. The key point of this approach consists in the representation theorem for groups $\mathcal{G}$ whose symmetry operations commute with the operator to be diagonalized, say $\mathcal{H}$. This theorem states that a basis for an irreducible representation of $\mathcal{G}$ is provided by the degenerate eigenvectors of $\mathcal{H}$ (see Chap. 6 of Ref. 21). In this respect, finding the spectrum of $\mathcal{H}$ is equivalent to block diagonalizing (i.e., reducing) the representations of $\mathcal{G}$ and its subgroups. We discuss here two specific atomic arrangements which frequently appear in the study of periodic systems: the simple-cubic and the face-centered-cubic lattices.

1. Simple-cubic lattice

In this system atoms are placed on the vertices of a cube of side a. The reciprocal elementary vectors are $\{\mathbf{b}_1, \mathbf{b}_2, \mathbf{b}_3\} = \frac{2\pi}{a}\{\hat{x}, \hat{y}, \hat{z}\}$ and the first Brillouin zone is a cube of side $2\pi/a$ [Fig. 1(a)]. We begin by discussing the group of wave vectors $\mathcal{G}(\mathbf{k})$ of high-symmetry points of the Brillouin zone. The space group is defined as the set of rotations and/or translations which keep the cubic lattice unchanged, or equivalently, which commutes with $\mathcal{L}_H$. Since the cubic lattice is characterized by a *symmorphic* space group (i.e., it does not commute with *screw* or *glide* operations given by noninteger translations of $\mathbf{a}$), the group of wave vectors is equivalent to a point group.[21] Table I reports the group of wave vectors of high-symmetry points of the Brillouin zone. Figure 1 displays $\omega(\mathbf{k})$ for the simple-cubic (SC) lattice. Owing to the small dielectric modulation ω_α^2/ω^2, $\omega(\mathbf{k})$ can be

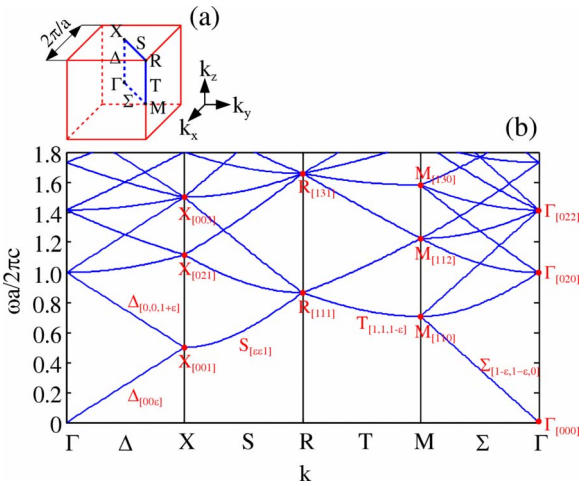

FIG. 1. (Color online) (a) First Brillouin zone and (b) x-ray dispersion relation of a SC lattice in the case of an infinitesimal periodic modulation. High-symmetry points are indicated with their reduced wave vector $\mathbf{k}\pi/a$.

constructed from the free-space relation $\omega(\mathbf{k})=c|\mathbf{k}|$ folded over itself at each $\mathbf{G}$ to fulfill Bloch theorem $\omega(\mathbf{k})=\omega(\mathbf{k}+\mathbf{G})$. As seen, no band gaps open in the wave spectrum and Bloch modes exist for all frequencies ω. Each $\mathbf{k}$ point defines a set of degenerate plane waves which possess the same eigenfrequency $\omega(\mathbf{k})$ in the absence of periodicity. If properly combined, these waves form a basis for Bloch modes, the expression of which is provided by the theory of projection operators once $\mathcal{G}(\mathbf{k})$ is reduced to a combination of irreducible representations. Table II reports the irreducible representations of high-symmetry points in the first Brillouin zone, whereas Table III presents expressions of z-propagating magnetic Bloch modes for $\omega a/2\pi c<1$ (e.g., for $\lambda>a$). As observed, the latter are doubly degenerate (i.e., they are polarized along either x or y). This is a general result and depends on the fact that Bloch modes are constructed from degenerate eigenwaves of the free space; hence, their polarization belongs to the transverse plane (x,y).

2. Face-centered-cubic lattice

In a face-centered-cubic (fcc) lattice, atoms are placed on both vertices and faces of a cube of side $a\sqrt{2}$. The elementary

TABLE I. Group of wave vectors $\mathcal{G}(\mathbf{k})$ calculated for high-symmetry points of a SC lattice.

Point	$\mathbf{k}\pi/a$	$\mathcal{G}(\mathbf{k})$
Γ	$[0,0,0]$	O_h
Δ	$[0,0,\epsilon]$	D_{4h}
X	$[0,0,1]$	D_{4h}
S	$[\epsilon,\epsilon,1]$	C_{2v}
R	$[1,1,1]$	O_h
T	$[1,1,1-\epsilon]$	C_{4v}
M	$[1,1,0]$	D_{4h}
Σ	$[1-\epsilon,1-\epsilon,0]$	C_{2v}

TABLE II. Reduction to irreducible representations of the group of wave vectors $\mathcal{G}(\mathbf{r})$ for various points of the reciprocal space of a SC lattice.

Point[a]	Irreducible representation of $\mathcal{G}(\mathbf{k})$ [b]
$\Gamma_{[000]}$	T_{1u}
$\Delta_{[0,0,\epsilon]}$	E
$X_{[0,0,1]}$	E_g+E_u
$S_{[\epsilon,\epsilon,1]}$	$A_1+A_2+B_1+B_2$
$R_{[1,1,1]}$	$E_g+E_u+T_{1g}+T_{1u}+T_{2g}+T_{2u}$
$T_{[1,1,1-\epsilon]}$	$A_1+A_2+B_1+B_2+2E$
$M_{[1,1,0]}$	$A_{2g}+A_{2u}+B_{1g}+B_{1u}+E_g+E_u$
$\Sigma_{[1-\epsilon,1-\epsilon,0]}$	B_1+B_2
$\Delta_{[0,0,1+\epsilon]}$	E

[a]High-symmetry points are indicated with the reduced wave vector $\mathbf{k}\pi/a$.
[b]We label representations according to the Mulliken notation (Ref. 21).

vectors are $\mathbf{b}_1=\frac{2\pi}{a}[-1,1,1]$, $\mathbf{b}_2=\frac{2\pi}{a}[1,-1,1]$, and $\mathbf{b}_3=\frac{2\pi}{a}[1,1,-1]$, while the first Brillouin zone is a truncated octahedron of height $4\pi/a$ [Fig. 2(a)]. Table IV shows the group of wave vectors $\mathcal{G}(\mathbf{k})$ for high-symmetry points in $\mathbf{k}$ space as well as their irreducible representations. Figure 2 displays the dispersion relation for the fcc lattice, with high-symmetry points indicated with the reduced wave vector $\mathbf{k}2\pi/a$. Finally, Table V shows the magnetic Bloch modes for the same conditions assumed for the SC lattice. As seen, due to the same symmetry group possessed by Δ and X points in the fcc and SC lattices, Bloch modes have identical expressions in these two systems.

C. Reduction through Bloch-mode expansion

Once the spectrum $\mathcal{S}$ of the canonical structure is known, the reduction of Eq. (1) is performed by exploiting the following identity [we let $\mathbf{e}=\mathbf{E}\exp(-i\omega t)+\text{c.c.}$ and $\mathbf{h}=\mathbf{H}\exp(-i\omega t)+\text{c.c.}$]:

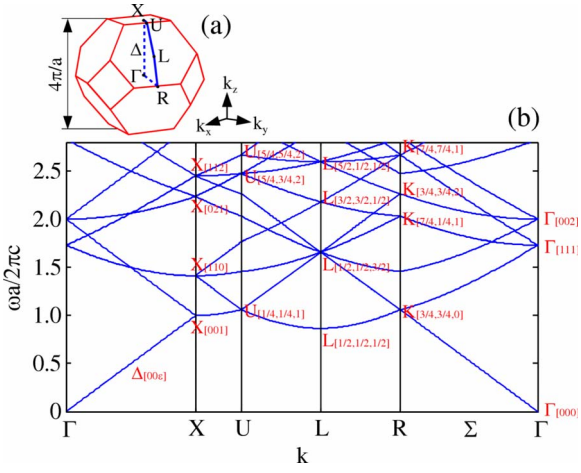

FIG. 2. (Color online) (a) First Brillouin zone and (b) x-ray electromagnetic band structure for a fcc lattice.

TABLE III. Expression of Bloch modes for high-symmetry points of the Brillouin zone of a simple-cubic lattice.

Point	Representation	Bloch mode $\mathbf{H}_{\mathbf{k}}$
$\Delta_{[0,0,\epsilon]}$	E	$\begin{Bmatrix}\hat{\mathbf{x}}\exp[i\pi/a(\epsilon z)]\\ \hat{\mathbf{y}}\exp[i\pi/a(\epsilon z)]\end{Bmatrix}$
$X_{[0,0,1]}$	E_g	$\begin{Bmatrix}\hat{\mathbf{x}}\sin(\pi/az)\\ \hat{\mathbf{y}}\sin(\pi/az)\end{Bmatrix}$
$X_{[0,0,1]}$	E_u	$\begin{Bmatrix}\hat{\mathbf{x}}\cos(\pi/az)\\ \hat{\mathbf{y}}\cos(\pi/az)\end{Bmatrix}$
$\Delta_{[0,0,\epsilon+1]}$	E	$\begin{Bmatrix}\hat{\mathbf{x}}\exp[i\pi/a(\epsilon z)]\\ \hat{\mathbf{y}}\exp[i\pi/a(\epsilon z)]\end{Bmatrix}$

$$\nabla\cdot(\mathbf{E}\times\tilde{\mathbf{H}}^{*}+\tilde{\mathbf{E}}^{*}\times\mathbf{H})+\mathbf{j}_{\Delta}\cdot\tilde{\mathbf{E}}^{*}=0. \tag{7}$$

Equation (7) is a form of the reciprocity theorem of Maxwell equations[24] and does not contain any approximation, as it can be verified by direct substitution. It allows the derivation of an exact evolution equation for the field. We begin by calculating the relationship between the current shift $\mathbf{j}_{\Delta}$ and $\mathbf{E}$ and $\mathbf{H}$. To this aim, we solve the plasma fluid equations by an iterative expansion in the field components:

$$n=n_0+n^{(1)}e^{-i\omega t}+n^{(2)}e^{-2i\omega t}+\text{c . c.},$$

$$\mathbf{v}=\mathbf{V}^{(1)}e^{-i\omega t}+\mathbf{V}^{(2)}e^{-2i\omega t}+\text{c . c.} \tag{8}$$

The overall current contribution with frequency ω can be written as

$$\mathbf{j}=[\mathbf{j}^{(1)}+\mathbf{j}^{(3)}]e^{-i\omega t}, \tag{9}$$

where

$$\mathbf{j}^{(1)}=\mathbf{j}_L=(iq^2n_0/\omega m)\mathbf{E},$$

$$\mathbf{j}^{(3)}=-qn^{(2)}[\mathbf{V}^{(1)}]^{*}-q[n^{(1)}]^{*}\mathbf{V}^{(2)}, \tag{10}$$

the latter accounting for the third-order nonlinearity. By substituting Eqs. (8)–(10) into the last two equations in Eq. (1), we obtain after straightforward algebra

$$\mathbf{V}^{(1)}=\frac{-iq}{\omega m}\mathbf{E},\quad n^{(1)}=-\frac{q}{\omega^2 m}\nabla n_0\cdot\mathbf{E}, \tag{11}$$

$$\mathbf{V}^{(2)}=\frac{iq^2}{4\omega^3m^2}\nabla\mathbf{E}^2, \tag{12}$$

$$n^{(2)}=\frac{q^2}{2\omega^4m^2}\left[\nabla\cdot(\mathbf{E}^2\nabla n_0)+\frac{1}{4}\nabla\cdot(n_0\nabla\mathbf{E}^2)\right], \tag{13}$$

with $\mathbf{E}^2\equiv\mathbf{E}\cdot\mathbf{E}$. The nonlinear current oscillating at ω is therefore expressed as

TABLE IV. Group of wave vectors $\mathcal{G}(\mathbf{k})$ calculated for high-symmetry points of a fcc lattice.

Point[a]	$\mathcal{G}(\mathbf{k})$	Irreducible representation
$\Gamma_{[0,0,0]}$	O_h	T_{1u}
$\Delta_{[0,0,\epsilon]}$	D_{4h}	E
$X_{[0,0,1]}$	D_{4h}	E_g+E_u
$S_{[\epsilon,\epsilon,1]}$	C_{2v}	$A_1+A_2+B_1+B_2$
$U_{[1/4,1/4,1]}$	C_{2v}	$A_1+A_2+2B_1+2B_2$
$L_{[1/2,1/2,1/2]}$	D_{3d}	E_g+E_u
$K_{[3/4,3/4,0]}$	C_{2v}	$A_1+A_2+2B_1+2B_2$
$\Sigma_{[\epsilon,\epsilon,0]}$	C_{2v}	B_1+B_2

[a]High-symmetry points are indicated with the reduced wave vector $\mathbf{k}2\pi/a$.

$$\mathbf{j}^{(3)}=-i\frac{q^4}{2\omega^5m^3}\mathbf{E}^{*}\left[\nabla\cdot(\mathbf{E}^2\nabla n_0)+\frac{1}{4}\nabla\cdot(n_0\nabla\mathbf{E}^2)\right]+i\frac{q^4}{4\omega^5m^3}[\nabla n_0\cdot\mathbf{E}]\nabla\mathbf{E}^2. \tag{14}$$

The second-order current contribution oscillating at 2ω, which contains terms with the products of $n^{(1)}\mathbf{V}^{(1)}$ and $n_0\mathbf{V}^{(2)}$, can be neglected as far as the input direction does not satisfy phase-matching conditions;[14] correspondingly, the phase effect in the forward scattering is negligible.

In the following we will focus on the direct beam by retaining only those terms inducing self-phase modulation in the input propagation direction. The reason for this choice is twofold:

(i) In the final expression of $\mathbf{j}$, Eq. (14), the terms including ∇n_0, accounting for the nonlinear Bragg scattering at directions other than the propagation direction of the incident beam, are quite small (they depend on the modulation of n_0). Nonlinear dynamical effects associated with these terms require a much higher intensity with respect to terms describing scattering parallel to the input direction;

(ii) Our findings are not limited to periodical samples but can be extended to the nonperiodic case; indeed the features of the crystal lattice mainly influence diffracted orders, while the nonlinear effects on the forward propagating beam are expected to be observed for samples with comparable spatially averaged charge density $\langle n_0\rangle$.

TABLE V. Expression of Bloch modes for high-symmetry points of the Brillouin zone of a fcc lattice.

Point	Representation	Bloch mode $\mathbf{H}_{\mathbf{k}}$
$\Delta_{[0,0,\epsilon]}$	E	$\begin{Bmatrix}\hat{\mathbf{x}}\exp[i\pi/a(\epsilon z)]\\ \hat{\mathbf{y}}\exp[i\pi/a(\epsilon z)]\end{Bmatrix}$
$X_{[0,0,1]}$	E_g	$\begin{Bmatrix}\hat{\mathbf{x}}\sin(\pi/az)\\ \hat{\mathbf{y}}\sin(\pi/az)\end{Bmatrix}$
$X_{[0,0,1]}$	E_u	$\begin{Bmatrix}\hat{\mathbf{x}}\cos(\pi/az)\\ \hat{\mathbf{y}}\cos(\pi/az)\end{Bmatrix}$

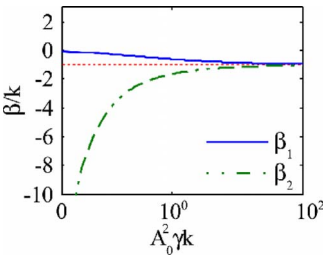

FIG. 3. (Color online) Solution of nonlinear dispersion relation (17): The continuous (dashed-dotted) line is the forward (backward) propagating wave; the horizontal dashed line corresponds to the asymptotic value $k_{nl}=-k$.

We therefore retain only longitudinal scattering terms in Eq. (13) and obtain

$$\mathbf{j}^{(3)} = \frac{-iq^4\langle n_0\rangle}{8\omega^5 m^3}\mathbf{E}^*\nabla^2\mathbf{E}^2. \tag{15}$$

We consider a z-propagating beam with frequency below the first turning point of the band structure (see Fig. 2 for $a/\lambda < 1$); in this case the treatment is simplified by the fact that only one Bloch function is involved. By exploiting Table III, the field can be written as

$$\mathbf{E} = \sqrt{2\eta_0}A(z)\hat{\mathbf{y}}e^{ikz}, \quad \mathbf{H} = -\sqrt{2/\eta_0}A(z)\hat{\mathbf{x}}e^{ikz}, \tag{16}$$

where $\eta_0=\sqrt{\mu_0/\epsilon_0}$ is the vacuum impedance. Bloch functions are normalized such that $4|A(z)|^2$ yields the beam intensity; correspondingly, Eq. (7) becomes

$$\frac{dA}{dz} = i\gamma A^* e^{-2ikz}\frac{d^2}{dz^2}(A^2e^{2ikz}), \tag{17}$$

where $\gamma=\eta_0^2q^4\langle n_0\rangle/8m^3\omega^5$. We remark that Eq. (17) differs from the standard self-phase modulation (SPM) equation (see, e.g., Ref. 16) and holds true for rapidly varying amplitudes $A(z)$.

D. Nonlinear waves

Equation (17) is integrable and its solution is found as $A(z)=A_0\exp(ik_{\mathrm{nl}}z)$, where k_{nl} is the nonlinear contribution to the wave vector satisfying

$$k_{\mathrm{nl}} + \frac{q^4\eta_0^2A_0^2}{2\omega^5m^3}(k+k_{\mathrm{nl}})^2 = 0. \tag{18}$$

Equation (18) always has two real-valued solutions, as shown in Fig. 3. At variance with standard SPM, the largest solution (continuous line in Fig. 3) does not linearly grow with the power A_0^2 and asymptotically tends to $-k$ from above. This wave is forward propagating. Conversely, the other solution provides $k+k_{\mathrm{nl}}<0$ (dashed-dotted line in Fig. 3), representing a backward propagating wave. These two solutions at large powers have the same wave vector; this can involve a nonlinear coupling between them, which strongly relies on the material lattice and will be considered in future work.

The stability of the two nonlinear waves is found by adding a small perturbation a_1 to the solution,

$$A(z) = [A_0 + a_1(z)]\exp(ik_{\mathrm{nl}}z), \tag{19}$$

with $a_1(z)$ as a complex-valued function. At the lowest order in $a_1(z)$, we obtain

$$2\gamma A_0^2\frac{d^2a_1}{dz^2} + i[1+8\gamma A_0^2(k+k_{\mathrm{nl}})]\frac{da_1}{dz} + a_1 \times[k_{\mathrm{nl}} + 8A_0^2(k+k_{\mathrm{nl}})^2\gamma] + 4\gamma(k+k_{\mathrm{nl}})^2a_1^* = 0. \tag{20}$$

While looking for exponentially amplified solutions $a_1 \propto \exp(\alpha z)$, straightforward algebra leads to the conclusion that α is zero or purely imaginary for any value of A_0. The found solutions are therefore always stable.

E. Nonlinear Kerr index n_2 and the classical electron power

The existence of stable nonlinear plane waves allows us to identify an effective refractive index n, which depends on the beam intensity. The coefficient n can be written as

$$n = 1 - \delta/2 + i\sigma + k_{\mathrm{nl}}/k, \tag{21}$$

where σ is the absorption coefficient. The last term k_{nl}/k in Eq. (21) accounts for the nonlinear wave vector and, at the lowest order in the intensity, for the forward propagating solution, it reads

$$k_{\mathrm{nl}}/k = -|n_2|I = -\gamma kI, \tag{22}$$

with $n_2=-k\gamma<0$ as the effective Kerr coefficient. To determine the values of I for which nonlinear effects become relevant, a noticeable figure of merit is the ratio between n_2I and $\delta/2$ that, after simple algebra, is written as

$$\mathcal{N} \equiv \frac{2|n_2|I}{\delta} = \frac{1}{4\pi}\frac{\lambda^2 I}{P_0}, \tag{23}$$

where $P_0=mc^3/r_0\cong 8.8$ GW is the *classical electron power* and $r_0=q^2/4\pi\epsilon_0mc^2$ is the electron radius. Equation (23) states that if a beam of power P_0 is focalized down to the diffraction limit (spot area on the order of $\lambda^2/2\pi$), then $\mathcal{N}\cong 0.5$; i.e., the plasma nonlinear contribution is of the same magnitude as the linear one. This implies that nonlinear effects could be observed in the current FLASH experiments at DESY (Refs. 6 and 18) (where $P\cong$ 10 GW) for tightly focused beams (waist $\approx$100 nm), and certainly they will be observable with the next generation of x-ray FELs.

F. Experimental realization and the role of losses

We estimate the magnitude of nonlinear effects in the direct beam propagation with reference to the simple case of beam self-defocusing. We consider a linearly polarized forward z-propagating beam with spatial profile $E\propto\exp(-r_\perp^2/w_0^2)$ focused onto a sample (here $r_\perp^2=x^2+y^2$ and w_0 is the beam waist). The field is expected to display a power-dependent divergence in the far field. For an input beam intensity such that

$$A_0^2(r_\perp) = I_0\exp\left(-\frac{2r_\perp^2}{w_0^2}\right), \tag{24}$$

the output beam acquires an additional transverse nonlinear phase profile given by

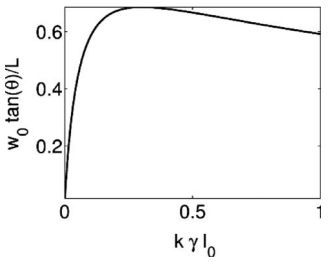

FIG. 4. Divergence vs input peak intensity I_0 in dimensionless units.

$$\Phi_{\rm nl}(r_\perp) = \beta[A_0(r_\perp)]L, \tag{25}$$

where L is the sample length. To the lowest order in the beam peak intensity I_0, the forward propagating solution of Eq. (18) gives

$$\beta \cong -4k^2\gamma A_0^2(r_\perp). \tag{26}$$

Since the most pronounced nonlinear effects are in the proximity of the beam axis, one has

$$\Phi_{\rm nl}(r_\perp) \cong -4k^2\gamma L I_0\left(1-\frac{2r_\perp^2}{w_0^2}\right), \tag{27}$$

which implies that the sample acts as an effective thin lens with negative focal length,

$$f = -\frac{w_0^2}{16k\gamma I_0 L}. \tag{28}$$

Correspondingly, the acquired divergence angle θ is given by

$$\tan(\theta) = \frac{w_0}{|f|} = \frac{16k\gamma I_0 L}{w_0}. \tag{29}$$

At any order in I_0, conversely, we have

$$|f| = \frac{2w_0^2\xi}{L(1+8\xi-\sqrt{1+16\xi})}, \tag{30}$$

where $\xi \equiv k\gamma I_0$. Therefore, the divergence $\tan(\theta)$ can be expressed as

$$\tan(\theta) = \frac{L(1+8\xi-\sqrt{1+16\xi})}{2w_0\xi}. \tag{31}$$

Note that for small θ one has

$$\theta w_0 = 16k\gamma I_0 L, \tag{32}$$

which implies that if the waist is reduced (e.g., I_0 is increased), θ increases (Fig. 4). For large ξ, $\tan(\theta)$ saturates at about $0.6L/w_0$, which defines the largest attainable divergence.

In the future generation of x-ray FELs, peak intensities on the order of 100 GW with source size of 60 μm and divergence of 3 μrad will be at our disposal.[3] A beam with wavelength in the range of 0.1–10 nm and intensity of $\approx 10^{22}$ W cm^{-2} (spot size $\approx$100 nm) displays a linear divergence on the order of 2 mrad. In order to have an observable nonlinear defocusing, in the following we determine the intensity needed to induce a comparable beam divergence. For small divergence angles, owing to the linear relationship $\theta w_0 = 16k\gamma I_0 L$ between I_0 and the sample length L, the intensity needed to acquire a nonlinear divergence greater than the linear one is independent of the beam waist; this figure is therefore a good indicator for quantifying nonlinear effects. In real materials the available effective length for the self-defocusing is compelled by photoelectric absorption and/or other material losses, whose strength strongly depends on the atomic number Z. In order to account for these effects, we consider the intensity needed to obtain a divergence comparable with the linear one on the sample characteristic loss length, which is determined by two leading mechanisms: absorption [Figs. 5(a) and 5(b)] and electron-ion collisions [Figs. 6(a) and 6(b)] (electron-electron collisions are known to be negligible).[4] Figure 5(a) displays the intensity needed to induce a nonlinear divergence of 2 mrad for waist w_0 = 100 nm (or equivalently 20 mrad and for w_0 = 10 nm) by including material absorption, the latter quantified in terms of the characteristic absorption length of the considered media,[25] as displayed in Fig. 5(b). We estimated the average density of electrons as

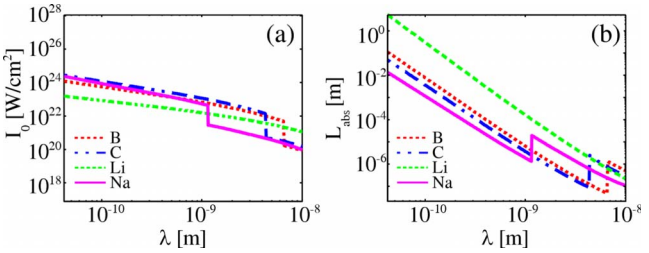

FIG. 5. (Color online) (a) Atomic-loss-limited intensity for nonlinear defocusing and (b) material absorption length versus wavelength.

$$\langle n_0\rangle = Z\mathcal{N}_a D M_m^{-1}, \tag{33}$$

where $\mathcal{N}_a$ is the Avogadro number, D is the material density, and M_m is the molar mass, thus obtaining $\langle n_0\rangle \cong 10^{30}$ m^{-3} for all of the considered materials. Figure 6(a) deals with electron-ion collisions described by the conductivity $\sigma_{\rm coll} = 3(KT)^{3/2}/2Z\sqrt{m/3}\pi q^2$, where K is the Boltzmann constant and T is the plasma temperature. The effects of the absorption due to electron-ion collisions give the absorption length reported in Fig. 6(b). By comparing Figs. 5 and 6, one finds

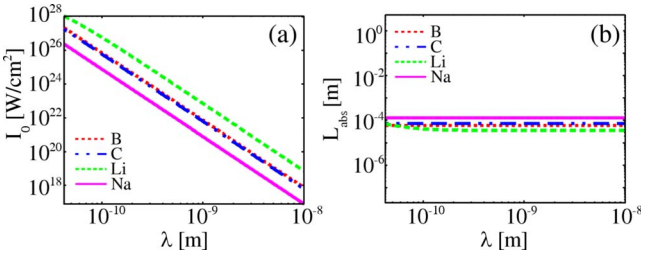

FIG. 6. (Color online) (a) Electronic-loss-limited intensity for nonlinear defocusing and (b) absorption length due to electron-ion collisions versus wavelength.

that electronic losses are dominant for wavelengths below 1 nm, while atomic losses govern the nonlinear dynamics for $\lambda > 1$ nm.

III. CONCLUSIONS

We predict that x-ray self-phase modulation is observable within the reported expected performances of future x-ray FEL sources for wavelengths of 1–10 nm and in the current FLASH experiments at DESY. Even if the diffraction limit (i.e., a beam waist comparable with the wavelength) is not reached, we find that as far as the involved powers are on the order of $P_0 = mc^3/r_0 \cong 10$ GW, if tightly focused beams are used for retrieving structural information (e.g., in the single molecule diffraction experiments), distortion due to nonlinear refraction is observable and influence the interpretation of the scattering pattern. This result is expected to be independent of the specific structure of the molecule.

[1] R. Dendy, *Plasma Physics: An in Introductory Course* (Cambridge University Press, Cambridge, 1996).

[2] T. Pfeifer, C. Spielmann, and G. Gerber, Rep. Prog. Phys. **69**, 443 (2006).

[3] Techical Design Report of the European XFEL, 2006, http://xfel.desy.de/tdr/tdr.

[4] H. Hora, *Physics of Laser Driven Plasmas* (Wiley, New York, 1981).

[5] R. Alkofer, M. B. Hecht, C. D. Roberts, S. M. Schmidt, and D. V. Vinnik, Phys. Rev. Lett. **87**, 193902 (2001).

[6] R. Moshammer *et al.*, Phys. Rev. Lett. **98**, 203001 (2007).

[7] H. Wabnitz, A. R. B. de Castro, P. Gurtler, T. Laarmann, W. Laasch, J. Schulz, and T. Moller, Phys. Rev. Lett. **94**, 023001 (2005).

[8] Y. Nabekawa, H. Hasegawa, E. J. Takahashi, and K. Midorikawa, Phys. Rev. Lett. **94**, 043001 (2005).

[9] T. Laarmann, A. R. B. de Castro, P. Gurtler, W. Laasch, J. Schulz, H. Wabnitz, and T. Moller, Phys. Rev. A **72**, 023409 (2005).

[10] E. P. Benis, D. Charalambidis, T. N. Kitsopoulos, G. D. Tsakiris, and P. Tzallas, Phys. Rev. A **74**, 051402(R) (2006).

[11] T. Sekikawa, A. Kosuge, T. Kanai, and S. Watanabe, Nature (London) **432**, 605 (2004).

[12] N. Bloembergen, R. K. Chang, S. S. Jha, and C. H. Lee, Phys. Rev. **174**, 813 (1968).

[13] S. S. Jha and C. S. Warke, Nuovo Cimento B **53**, 120 (1968).

[14] A. Nazarkin, S. Podorov, I. Uschmann, E. Forster, and R. Sauerbrey, Phys. Rev. A **67**, 041804(R) (2003).

[15] S. S. Jha and J. W. F. Woo, Phys. Rev. B **5**, 4210 (1972).

[16] N. Bloembergen, Proceedings of the IEEE, 1963, p. 124.

[17] R. W. Boyd, *Nonlinear Optics* (Academic, New York, 2003).

[18] R. Neutze, R. Wouts, D. van der Spoel, E. Weckert, and J. Hajdu, Nature (London) **406**, 752 (2000).

[19] Y. S. Kivshar and G. P. Agrawal, *Optical Solitons: From Fibers to Photonic Crystals* (Academic, San Diego, 2003).

[20] K. Sakoda, *Optical Properties of Photonic Crystals* (Springer-Verlag, Berlin, 2001).

[21] T. Inui, Y. Tanabe, and Y. Onodera, *Group Theory and Its Applications in Physics* (Springer-Verlag, Berlin, 1990).

[22] K. Sakoda, Phys. Rev. B **55**, 15345 (1997).

[23] J. Cornwell, *Group Theory and Electronic Energy Bands in Solids* (Wiley, New York, 1969).

[24] C. A. Balanis, *Advanced Engineering Electromagnetics* (Wiley, Toronto, 1989).

[25] *X-Ray Data Booklet*, edited by D. Vaughan (Lawrence Berkeley, Berkeley, CA, 1986).